JACS Au
AN OPEN ACCESS JOURNAL OF THE AMERICAN CHEMICAL SOCIETY

pubs.acs.org/jacsau

Article

Electrolysis Can Be Used to Resolve Hydrogenation Pathways at Palladium Surfaces in a Membrane Reactor

Aoxue Huang, Yang Cao, Roxanna S. Delima, Tengxiao Ji, Ryan P. Jansonius, Noah J. J. Johnson, Camden Hunt, Jingfu He, Aiko Kurimoto, Zishuai Zhang, and Curtis P. Berlinguette*

Cite This: *JACS Au* 2021, 1, 336–343

Read Online

ACCESS | Metrics & More | Article Recommendations | Supporting Information

ABSTRACT: For common hydrogenation chemistries that occur at high temperatures (where H_2 is adsorbed and activated at the same surface which the substrate must also adsorb for reaction), there is often little consensus on how the reactions (e.g., hydro(deoxy)genation) actually occur. We demonstrate here that an electrocatalytic palladium membrane reactor (ePMR) can be used to study hydrogenation reaction mechanisms at ambient temperatures, where the catalyst does not necessarily undergo structural reorganization. The ePMR uses electrolysis and a hydrogen-selective palladium membrane to deliver reactive hydrogen to a catalyst surface in an adjacent compartment for reaction with an organic substrate. This process forms the requisite metal-hydride surface for hydrogenation chemistry, but at ambient temperature and pressure, and without a H_2 source. We demonstrate the utility of this analytical tool by studying the hydrogenation of benzaldehyde at palladium nanocubes with dimensions of 13−24 nm. This experimental design enabled us to resolve that the alcohol product forms at the facial sites, whereas the hydrodeoxygenation step occurs at edge sites. These observations enabled us to develop the first site-specific definition of how a carbonyl species undergoes hydro(deoxy)genation.

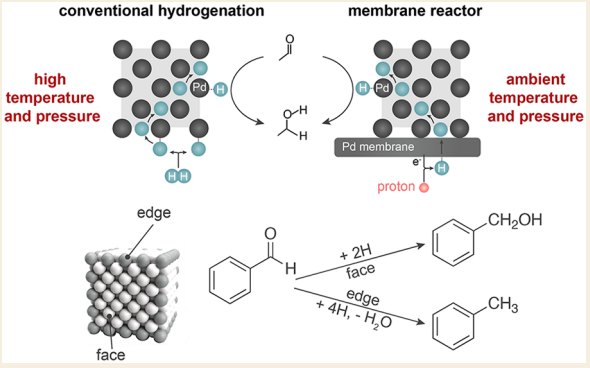

KEYWORDS: *palladium membrane reactor, hydrogenation, palladium nanocubes, benzaldehyde, catalytic mechanism, reaction pathways*

INTRODUCTION

Heterogeneous catalytic hydrogenation is relevant to the production of numerous fine[1] and bulk[2] chemicals and remains the primary method of hydrogenation on the industrial scale. The most commonly used catalysts for industrial-scale hydrogenation are based on high surface-area platinum group metals (PGMs), such as Pd/C and Pt black.[3] The wide use of these PGM catalysts motivates the need to clearly define how hydrogenation reactions occur at the surface of these catalysts.[4] Given that the structures of these catalysts are often ill-defined, previous mechanistic studies have utilized PGM nanocatalysts of differing sizes and shapes as a platform to develop structure−property relationships for hydrogenation. This strategy enables the ratio of relevant active sites (i.e., face, edge, and vertice) to be manipulated,[5−9] thereby offering a means of identifying site-specific hydrogenation pathways and providing design principles for industrially relevant PGM catalysts.[10,11]

The hydrogenation of organic carbonyl compounds at PGM catalysts can follow different reaction pathways,[12] and thus, a number of strategies have been used to manipulate reaction rates and product selectivities.[13−17] Despite extensive efforts to probe the reaction pathways of carbonyl hydrogenation through catalyst design alone, it remains difficult to assign reaction steps to specific catalytic sites because substrate binding, surfactant, and support effects[18] confound the influence of nanoparticle morphology on the reaction. For example, Pang et al. used self-assembled monolayers of alkanethiolates to control the availability of specific sites thereby directing furfural hydrogenation toward different products.[19] Zhang et al. used atomic layer deposition to cover the step sites of Pd particles on a Pd/Al_2O_3 support to increase the selectivity for furan during the hydrogenation of furfural.[20] These studies highlight how the surface adsorbents, catalyst morphology, and effects of catalyst support[18] all affect the reaction pathway. Deconvolution of these different factors is especially important when studying carbonyl substrates, which demonstrate a greater number of binding modes (e.g., η^1-(O), η^2-(C, O), η^1-(C)) and reaction pathways compared to alkenes and alkynes.[12,21] Additionally, competing reactions such as deoxygenation and decarbonylation and a wide range

Received: October 13, 2020
Published: February 26, 2021

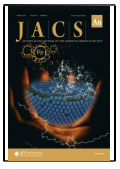

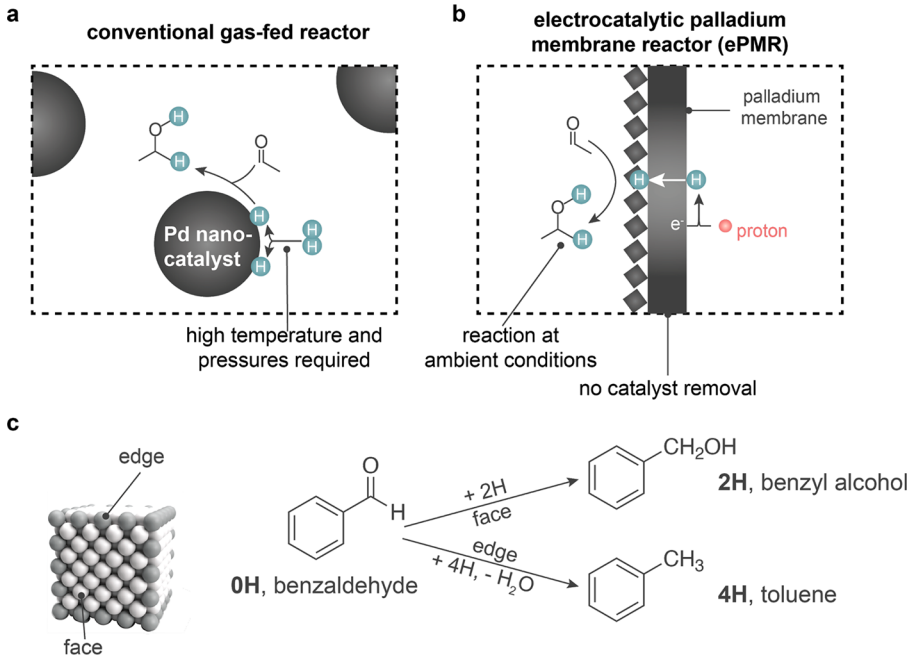

Figure 1. Schematic depiction of hydrogenation configurations and reaction pathways studied in this work. (a) Traditional gas-fed reactor for hydrogenation with Pd nanocatalysts. High temperature and pressure are required to enable reaction resulting in H_2 gas dissociation and reaction with C═O to form a hydrogenated product. (b) Electrocatalytic palladium membrane reactor (ePMR) for hydrogenation with a Pd membrane/catalyst. An applied current enables proton reduction to monatomic hydrogen. These monatomic hydrogen then permeates the Pd membrane to the other side to react with C═O to form a hydrogenated product. The ePMR provides a platform for tunable hydrogen content, reactions at ambient conditions, and no catalyst removal after reaction. (c) Proposed two-site reaction pathway of the hydrogenation of benzaldehyde (0H) to benzyl alcohol (2H) and toluene (4H) on the Pd nanocube facial and edge (edge is defined as edge and vertex) sites of the nanocube.

of possible nonredox side reactions have limited a detailed mechanistic understanding of carbonyl hydrogenation on PGM surfaces.[21] Moreover, C═O hydrogenation requires high reaction temperatures, which can induce structural changes of the catalyst during the reaction that complicates mechanistic studies.[22−24] A consequence of these experimental challenges is that there exists no universally accepted reaction mechanism for carbonyl hydrogenation on PGM surfaces.[21,25] Fundamentally different approaches are needed that allow for precise control of catalyst morphology, substrate delivery, and reaction conditions.

Central to our approach was the use of well-defined, size-dependent Pd nanocatalysts which serve as a materials platform to identify site-specific reaction pathways for carbonyl hydrogenation. These nanoparticles are uniform in their sizes and shapes based on the transmission electron microscopy (TEM) images and consist of distinctive face and edge sites to catalyze hydrogenation reactions. The precise manipulation of nanoparticle sizes enables the control of the ratio of different reaction sites to reveal the real mechanism of site-dependent hydrogenation reaction pathways. We paired these catalysts with our electrocatalytic palladium membrane reactor (ePMR), which not only enables hydrogenation at ambient temperatures and pressures but also provides acute control of the amount of hydrogen delivered to the reaction sites.[26,27] Together, this catalyst and reactor system addresses all of the previously discussed challenges and enables site-specific carbonyl hydrogenation reaction pathways for Pd to be elucidated (Figure 1).

The ePMR consists of an electrochemical compartment and a hydrogenation compartment separated by a Pd foil membrane. A key feature of this design is that the Pd membrane simultaneously acts as (i) a cathode to reduce protons in the electrochemical compartment into reactive H atoms; (ii) a membrane that selectively allows H atoms to migrate from the electrochemical compartment to the hydrogenation compartment for reaction; and (iii) a solid support for nanocatalysts (on the foil facing the hydrogenation compartment) that can react with substrates. In the electrochemical compartment, protons are electrochemically reduced into surface-adsorbed hydrogen at the Pd foil. These hydrogen atoms are easily absorbed into the interstitial sites of the Pd lattice[28] and permeate through the Pd membrane into the hydrogenation compartment to react with unsaturated bonds of species bound to the surface of the nanocatalyst. This architecture is useful for studying reaction mechanisms because it circumvents issues associated with low H_2 solubility in common solvents, allows for fine control over the supply of reactive H atoms (hydrogen flux) to the nanocatalyst with applied current,[26] and also removes the need to activate and adsorb H_2 at the Pd surface which complicates mechanistic studies.[29]

This study showcases the power of using an ePMR platform to study hydrogenation by investigating the conversion of benzaldehyde (0H) to form benzyl alcohol (2H) or toluene (4H). Depositing well-defined Pd nanocubes as the hydrogenation catalyst on the Pd membrane (facing the hydrogenation compartment) enabled us to quantify differences in hydrogenation chemistry at edge and vertex sites (collectively referred to as "edge" sites herein) from those that occur at facial sites (Figure 1c). We show that formation of 2H and 4H depends on the site at which the reaction occurs: 2H is produced at facial sites with first-order kinetics, while 4H is produced at edge sites with zero-order kinetics. It would have been challenging to determine this reaction chemistry using a

https://dx.doi.org/10.1021/jacsau.0c00051
JACS Au 2021, 1, 336−343

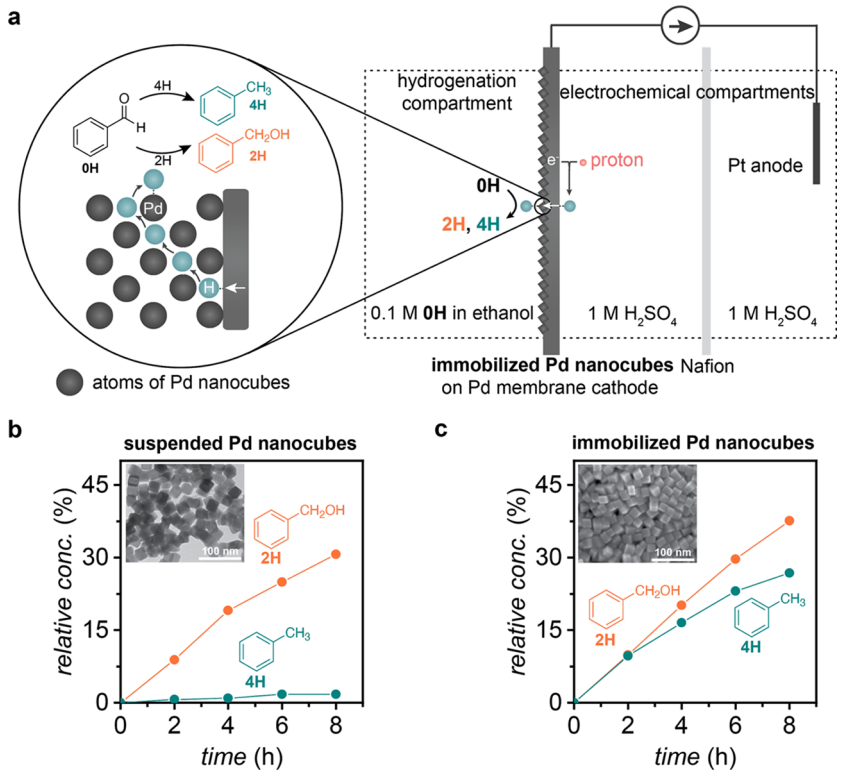

Figure 2. Electrocatalytic palladium membrane reactor (ePMR) designed for studying Pd nanocubes. (a) Schematic diagram of the three-compartment cell for performing hydrogenation with immobilized Pd nanocubes drop-cast on a bare Pd foil. A Nafion membrane separates the two electrochemical compartments and the Pd foil membrane separates the hydrogenation and electrochemical compartments. A current applied across the Pt anode and Pd cathode forms protons that are reduced to monatomic hydrogen on the Pd cathode surface. This monatomic hydrogen permeates the Pd foil, and the Pd nanocubes to react with benzaldehyde (0H) in the hydrogenation compartment. Hydrogenation of 0H to benzyl alcohol (2H) and toluene (4H) in ethanol for (b) suspended Pd nanocubes stirred in the hydrogenation compartment and (c) immobilized Pd nanocubes on the Pd membrane. Note: data in (b) is obtained using a bare Pd cathode/membrane without drop-cast Pd nanocubes. Inset of (b) shows a TEM image of $Cube_{24}$ after 24 h of reaction, and inset of (c) shows an SEM image of $Cube_{24}$ immobilized on Pd foil.

conventional setup of stirred suspension of a nanocatalyst due to high reaction temperature and the interference of surfactants. Nanocatalysts without surfactants tend to aggregate and precipitate from suspension.[30] However, the introduction of surfactants may reduce the accessibility of catalytic sites and complicate the interpretation of obtained kinetic data.[31−34] We were able to define the reaction pathways of C═O hydrogenation on Pd for the first time for two reasons: (i) Carbonyl hydrogenation can take place at room temperature in ePMR,[35] and thus, the sizes and shapes of the nanoparticle are retained over the course of the reactions. (ii) The surfactants on Pd nanoparticles are removed without destabilizing the reaction kinetics because the catalyst is structurally supported by the Pd membrane.

RESULTS

Experimental Apparatus

The ePMR used in this study consists of a three-compartment cell with a Pd foil used as both a cathode and a membrane for separating the hydrogenation and electrochemical reactions (Figures 2a and S1).[26] A proton-conducting Nafion membrane was used to separate the outer electrochemical compartment containing a Pt mesh anode from the middle electrochemical compartment containing a Ag/AgCl reference electrode and the Pd foil cathode. For all experiments, the middle and outer electrochemical compartments were filled with 35 and 45 mL of 1 M H_2SO_4, respectively. Benzaldehyde (0H) was selected as a model compound here because its analogues are used in the production of aromatic alcohol and upgrading processes of bioderived oil.[36−38] The hydrogenation compartment was filled with 0.1 M 0H in 30 mL of ethanol and stirred at a constant rate of 600 rpm. A galvanostatic current (200 mA) applied between the Pt and Pd electrodes was used to drive water oxidation at the Pt anode and simultaneous proton reduction at the Pd cathode. At this current, 90 ± 5% (equivalent to a H_2 flow rate of 1.37 ± 0.08 sccm) of electrochemically produced monatomic hydrogen passed through the membrane into the hydrogenation compartment (based on measurements of H_2 evolution in each compartment using an atmospheric mass spectrometer). Reaction progress was monitored by characterizing 500 μL aliquots of the reaction mixture, removed throughout the duration of the experiment, and examined by ^{1}H NMR spectroscopy to provide relative concentrations versus time plots.

Synthesis and Characterization of Pd Nanocubes

The Pd nanocubes responsible for the hydrogenation catalysis in this study were synthesized using a bromide-assisted method[39,40] with a polyvinylpyrrolidone (PVP) stabilizer. Pd nanocubes with different sizes were prepared by varying the concentrations of the KBr capping agent (Figure S2). The size of the samples (reported as the average edge length measured by TEM) were 13.0 nm ($Cube_{13}$), 15.3 nm ($Cube_{15}$), 21.0 nm ($Cube_{21}$), and 24.4 nm ($Cube_{24}$) (Figure S3). The mass-per-volume concentration of nanocubes in their aqueous stock

https://dx.doi.org/10.1021/jacsau.0c00051
JACS Au 2021, 1, 336−343

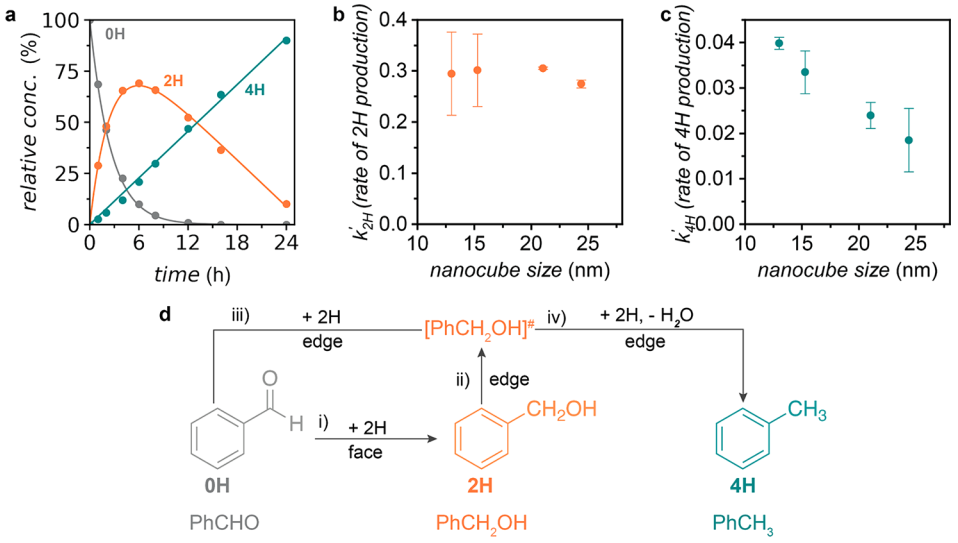

Figure 3. Effect of Pd nanocube size on benzaldehyde hydrogenation rates. (a) Sample concentration profile of the hydrogenation of benzaldehyde (0H) to benzyl alcohol (2H) and toluene (4H) using $Cube_{13}$. Kinetic fits were determined by finding best fits to eqs 1−3 for experimental data of $Cube_{13}$. An R^2 value of 0.998 was obtained. Relationship of effective rate constant and Pd nanocube size for (b) k'_{2H} (production of 2H) and (c) k'_{4H} (production of 4H). (d) Proposed reaction pathways of 2H and 4H on edge and facial reaction sites. The error bars in (b) and (c) are standard deviations calculated based on two independent prepared samples.

suspension were quantified by inductively coupled plasma optical emission spectroscopy (ICP-OES).

Pd nanocubes were studied as the hydrogenation catalyst in the hydrogenation compartment in two different configurations: (i) suspended Pd nanocubes or (ii) immobilized Pd nanocubes. For experiments with suspended Pd nanocubes, 1.77 mg of nanocubes was centrifuged from an aqueous stock suspension, dried under vacuum, redispersed in ethanol, and added to the reaction mixture in the hydrogenation compartment before current was applied. A bare Pd foil was used to supply hydrogen during these experiments. For immobilized Pd nanocubes, the aqueous suspension of nanocubes were used directly and drop-cast onto the hydrogenation side of the Pd foil with the same loading mass of 1.77 mg (geometric area = 1.77 cm^2). Unless stated otherwise, the drop-cast nanocubes were cleaned with sodium hydroxide to remove the PVP surfactant[41] before the drop-casting procedure. Fourier-transform infrared spectroscopy was used to prove that most PVP has been removed after the sodium hydroxide wash (Figure S4).

Benchmarking Immobilized Pd Nanocubes against Suspended Pd Nanocubes in the ePMR

The hydrogenation of 0H was first performed in the ePMR using the suspended $Cube_{24}$ in the hydrogenation compartment ("suspended Pd nanocubes"), with a bare Pd foil membrane. The same experiment was then performed with the immobilized $Cube_{24}$ deposited on the Pd foil facing the hydrogenation compartment ("immobilized Pd nanocubes"), with no suspended $Cube_{24}$ added to the hydrogenation compartment (Figure 2a). The PVP surfactant was required to suppress precipitation of the suspended $Cube_{24}$ before the reaction was initiated, and was consequently used for both experiments.[42]

An applied current of 200 mA across the electrochemical compartment in the ePMR without any Pd nanocubes showed no conversion of 0H over 24 h of electrolysis (Figure S5). The same experiment with suspended $Cube_{24}$ in the hydrogenation compartment resulted in a significant increase in 2H (31 mol %) production after 8 h of reaction (Figure 2b). There was also a small amount of 4H (1.7 mol %) produced over this same period, as well as a side product (likely the diethyl acetal of 0H) that persisted at ∼25 mol % until the end of the experiment (Figures S6−S8). The suspended $Cube_{24}$ had almost fully precipitated out of the reaction mixture after 6 h of reaction (Figure S9).

The same experiment performed with immobilized $Cube_{24}$ generated 38 mol % 2H and 27 mol % 4H products over the 8 h time period. These values correspond to approximately the same amount of 2H formed as in the suspended $Cube_{24}$ but a striking 16-fold increase in 4H production. Moreover, the reactions with immobilized $Cube_{24}$ did not yield any acetal formation (Figure S7). Note that a separate experiment using the immobilized $Cube_{24}$ where the PVP surfactant was removed led to a doubled rate of hydrogenation of 0H. This increase was directed almost exclusively to the formation of 2H, as almost no increase in 4H production was observed over 24 h of reaction (Figure S10).

Hydrogenation Rate as a Function of Pd Nanocube Size

We then set out to study the effect of Pd nanocube size on selectivity and reactivity of benzaldehyde hydrogenation using the immobilized Pd nanocubes in the ePMR. The nanocube sizes that we tested were 13, 15, 21, and 24 nm in edge length ($Cube_{13}$, $Cube_{15}$, $Cube_{21}$, and $Cube_{24}$, respectively). At least two independently prepared samples were tested under identical conditions for each size. SEM images of the Pd nanocubes taken after 24 h of hydrogenation at 200 mA confirmed that the shape of the nanocubes was unchanged (Figure S11). The relative concentration of reactant (0H) and products (2H, 4H) monitored by ^{1}H NMR (Figure S12) over this time period exhibited similar trends for each of the four sizes. The concentration profiles showed that the relative concentration of 2H increased to a maximum of 60−80 mol % around t = 8 h before decreasing over the remainder of the 24 h reaction. The concentration profile of 4H revealed a very different trend, increasing linearly with time for all nanocube sizes. Moreover, a faster production of 4H was observed for

https://dx.doi.org/10.1021/jacsau.0c00051
JACS Au 2021, 1, 336−343

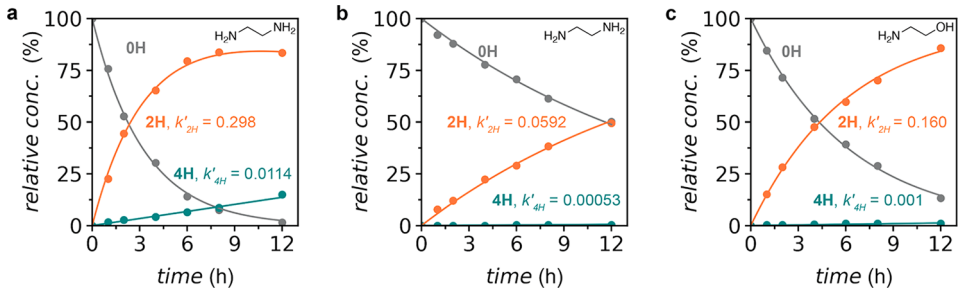

Figure 4. Effect of coordination agents on benzaldehyde hydrogenation rates. Concentration profiles of benzaldehyde (0H) to benzyl alcohol (2H) and toluene (4H) with (a) 0.002 mM ethylenediamine (NN), (b) 0.2 mM NN, and (c) 0.2 mM ethanolamine (NO). Kinetic fits were determined by finding the best fits for eqs 1−3 for experimental data of $Cube_{13}$.

progressively smaller nanocubes with the $Cube_{24}$ and $Cube_{13}$ samples producing 48 and 90 mol % 4H at t = 24 h, respectively (Figures 3a and S13).

The Coordination Effect of Ligands on Hydrogenation Rates

Previous work has shown that ethylenediamine (NN) can bind to Pd surfaces and suppress deoxygenation of benzaldehyde derivatives.[43] This work inspired us to test how this ligand would affect hydrogenation catalysis on immobilized Pd nanocubes. These experiments were conducted by adding NN into the hydrogenation compartment 2 h prior to carrying out each hydrogenation experiment (using immobilized $Cube_{13}$ as the catalyst). We also tested a structural similar, yet weaker, ligand ethanolamine (NO) under the same experimental conditions to evaluate any differences in reactivity. SEM images showed no catalyst deformation because the morphology of immobilized $Cube_{13}$ did not change after the hydrogenation in the presence of NN (Figure S14).

The addition of a low concentration of NN (0.002 mM) resulted in 15 mol % in 4H formation at t = 12 h (Figure 4a), only 1/3 the concentration of the unpoisoned experiment which exhibited 44 mol % (Figure 3a). The initial formation rate of 2H did not decrease significantly, resulting in an increased maximum concentration of 2H of 84 mol %, from the 69 mol % of unpoisoned experiments. With higher NN concentrations from 0.002 mM to 0.02 mM and 0.2 mM (Figures 4a,b and S15a), the productivity of 2H and 4H both decreased. The concentration of 4H at t = 12 h dropped from 15 mol % to 7 mol % and 0.3 mol %, respectively, and the production of 2H in the first hour of reaction went down from 23 mol % to 14 mol % and 8 mol %, respectively.

When 0.2 mM NO was added to the reaction vessel instead of NN, the reaction resulted in higher consumption of 0H after 12 h of reaction (Figure 4b,c). The 4H concentration at the end of the experiment was less than 1 mol % in both cases while the concentration of 2H was 36 mol % higher (86 and 50 mol % for NO and NN, respectively). The productivity of 2H was significantly improved with a small decrease of 2H selectivity, at t = 12 h from 99.3% with NN to 98.8% with NO in terms of the percentage of 2H in the products ([2H]/[2H + 4H]).

DISCUSSION

We report here how these advantages provided by the ePMR can yield unprecedented insight into reaction mechanisms. Using an ePMR containing a Pd membrane decorated with well-defined nanoparticles facing the hydrogenation compartment, we studied the hydrogenation of benzaldehyde (0H) to form benzyl alcohol (2H) and toluene (4H). We studied this prototypical reaction as a function of Pd nanocube size and added ligands. These experiments serve to correlate hydrogenation activity to the ratio of palladium edge sites to facial sites on the surface, and to define specific reaction sites during carbonyl hydrogenation.

We first compared the hydrogenation of 0H catalyzed by immobilized $Cube_{24}$ to those catalyzed by suspended $Cube_{24}$ in the ePMR. The immobilized $Cube_{24}$ highlighted 16-fold faster formation of 4H and 1.2-fold faster formation of 2H. This trend supports the notion that hydrogenation is faster without the competing H_2 adsorption and activation processes at the same surface, which must otherwise occur for hydrogenation on suspended Pd nanoparticles. We also note that the suspended $Cube_{24}$ showed signs of aggregation even with the PVP surfactant. This aggregation has been attributed to the removal of PVP surfactant by the hydride species formed during hydrogenation.[44] In sum, immobilizing Pd catalysts in the ePMR yields faster hydrogenation and avoids the complications of dealing with catalyst aggregation.

We then performed hydrogenation using four different sizes of immobilized Pd nanocubes and found that catalyst size does indeed influence the rate and selectivity of the reaction. Smaller nanocubes were found to mediate the faster formation of the hydrodeoxygenation product (4H), while larger ones lead to higher 2H peak concentrations. The mass transport limited reaction is estimated to take 2.2 h to go to 99% completion (see the Supporting Information) under the reaction conditions. In our experiments, it takes more than 12 h to go to 99% completion. On this basis, we contend our reaction is not limited by mass transport. Notably, the shape of the concentration profile of 4H and 2H as the function of time was similar (i.e., linear for 4H and quadratic for 2H) for all sizes of nanoparticles, suggesting the same hydrogenation pathways for 0H hydrogenation. The different evolution of 4H and 2H concentrations suggest that the two products may form on different catalytic sites. These inferences prompted us to build a kinetic model to better understand the hydrogenation pathways of 0H in our system.

The kinetic model we propose here (Figure 3d) assumes two distinct hydrogenation sites on the surface of a nanocube: facial and edge sites (vertex sites are not resolved from edge sites in this work because they account for less than 0.06% surface atoms). We built the kinetic model based on the following hypotheses: (i) at facial sites, 0H adsorbs and undergoes a fast 2H-reduction into 2H which then desorbs from the surface; (ii) 2H formed on facial sites can migrate to edge sites; (iii) at edge sites, adsorbed 0H undergoes a fast 2H-

https://dx.doi.org/10.1021/jacsau.0c00051
JACS Au 2021, 1, 336−343

reduction without releasing 2H; and (iv) the intermediate then undergoes a slow 2H-reduction to form 4H.

Based on this kinetic model, we proposed the integrated rate laws in eqs 1−3 with the following rationales. The formation of 4H is overall zero-order because it is limited by the number of edge sites available (edge sites represent <3% of surface atoms). The formation of 4H is constant whether it is reduced directly from 0H or from readsorbed 2H because both reactions share the same rate-limiting step. The formation of 2H is in direct correlation with the concentration of 0H and assumed to be first-order due to the abundance of facial sites. This model provided fits to the experimental data with $R^2 > 0.985$ for all nanocubes sizes (Table S1). Alternative to eqs 1−3, fittings with first-order kinetics show significant deviation from data (Figure S16b,c).

$$\frac{d[4H]}{dt} = k'_{4H} \tag{1}$$

$$\frac{d[0H]}{dt} = -k'_{2H}[0H] - k'_{4H}\frac{[0H]}{[0H] + [2H]} \tag{2}$$

$$\frac{d[2H]}{dt} = k'_{2H}[0H] - k'_{4H}\frac{[2H]}{[0H] + [2H]} \tag{3}$$

The extrapolated k'_{2H} and k'_{4H} revealed a clear correlation between the size of Pd nanocubes and preference for each reaction pathway. Electrochemical surface area measurements revealed that surface roughness was similar for every sample (Figure S17). Internal diffusion does not appear to influence reaction rates. When we increased the catalyst loading from 1.0 to 1.5 mg cm^{-2}, the concentration profiles were superimposed (Figure S18). The k'_{4H} doubled from $Cube_{24}$ to $Cube_{13}$ because the percentage of edge sites on the surface increased ~2-fold (from 1.58% to 2.95%), leading to more available edge sites per surface area (Table 1). The k'_{2H} is relatively independent of the nanocube size because the percentage of facial sites on is large for all samples (>97%) and effectively held at nearly parity.

Table 1. Percentage of Reactive Sites in Total Surface Atoms on Different Pd Nanocubes[a]

		ratio of reactive sites to surface atoms	
Pd nanocube	d_p (nm)	edge/N_S (%)	face/N_S (%)
$Cube_{13}$	13.00	2.95	97.05
$Cube_{15}$	15.28	2.52	97.48
$Cube_{21}$	21.03	1.83	98.17
$Cube_{24}$	24.39	1.58	98.42

[a] d_p is the average edge length, and N_S is the number of surface atoms.

The data from the ligand poisoning experiments also support our kinetic model. When the lowest concentration of NN was added to the reaction (0.002 mM corresponds to 1.36 equiv. of the total number of edge sites for $Cube_{13}$), k'_{4H} dropped 70% from that of the unpoisoned catalyst, and k'_{2H} only decreased by 15% (Figure S15b). We therefore assert that the large reduction in 4H production (k'_{4H}) compared to 2H (k'_{2H}) arises from the NN ligand efficiently poisoning the edge sites, forcing the reaction to proceed only at nanoparticle facial sites. The same effect was observed using the NO ligand, albeit to a lesser extent due to weaker binding to the Pd atoms, resulting in less pronounced deactivation of both edge and facial sites. Ligands are known to preferentially bind to sites with a lower coordination number.[45,46] Contrary to NN and NO ligands, we show that the polymeric surfactant PVP preferentially suppresses 2H formation (Figure S10). We, therefore, contend that PVP may not coordinate effectively to reactive sites but rather works by wrapping around Pd nanoparticles[34,47] and hindering the adsorption of substrate molecules. The 4H production rate was not noticeably impacted by PVP because the number of edge sites available for reaction was not affected.

CONCLUSIONS

We report here the site-specific reaction pathways for the hydrogenation of the aromatic carbonyl group. This study was only made possible by the design of Pd nanocatalysts with well-controlled sizes and shapes for use in the electrocatalytic palladium membrane reactor (ePMR). We have shown that reaction pathways in the hydrogenation of C═O compounds such as benzaldehyde (0H) can be deconvoluted by systematically changing the size of nanocatalyst and titrating the reactive sites with coordination ligands. Our results suggest that ethylenediamine (NN) ligands coordinate more strongly to sites with lower coordination numbers, resulting in a significant reduction in toluene (4H) production. This knowledge is not conveyed in literature, even though ethylenediamine (NN) ligands are widely used to inhibit the deoxygenation reactions.[43] We propose that smaller nanoparticles with a high density of edge sites be employed in applications where deoxygenation is desired (e.g., the production of biofuels from aromatic aldehydes[12,37]). We also expect that the ePMR combined with well-defined nanoparticles may enable hydrogenation of more difficult substrates.

ASSOCIATED CONTENT

Supporting Information

The Supporting Information is available free of charge at https://pubs.acs.org/doi/10.1021/jacsau.0c00051.

Experimental details; photograph of the three-compartment cell used as the ePMR; TEM images of the synthesized Pd nanocubes; Size distribution of $Cube_{13}$, $Cube_{15}$, $Cube_{21}$, and (d) $Cube_{24}$; 1H NMR spectra; Acetal formation over time for the hydrogenation of 0H in the suspended Pd nanocubes; photographs of suspended Pd nanocubes ($Cube_{24}$) during 0H hydrogenation; 0H hydrogenation with immobilized Pd nanocubes; SEM images; kinetic fitting of Pd nanocubes and kinetic data; FTIR spectra; ECSA of drop-cast nanocube samples (PDF)

AUTHOR INFORMATION

Corresponding Author

Curtis P. Berlinguette − *Department of Chemistry, Stewart Blusson Quantum Matter Institute, and Department of Chemical & Biological Engineering, The University of British Columbia, Vancouver, BC V6T 1Z1, Canada; Canadian Institute for Advanced Research (CIFAR), Toronto M5G 1M1, Ontario, Canada;* orcid.org/0000-0001-6875-849X; Email: cberling@chem.ubc.ca

https://dx.doi.org/10.1021/jacsau.0c00051
JACS Au 2021, 1, 336−343

Authors

Aoxue Huang − *Department of Chemistry, The University of British Columbia, Vancouver, BC V6T 1Z1, Canada*

Yang Cao − *Department of Chemistry and Stewart Blusson Quantum Matter Institute, The University of British Columbia, Vancouver, BC V6T 1Z1, Canada;* orcid.org/0000-0001-8636-7919

Roxanna S. Delima − *Stewart Blusson Quantum Matter Institute and Department of Chemical & Biological Engineering, The University of British Columbia, Vancouver, BC V6T 1Z4, Canada*

Tengxiao Ji − *Department of Chemistry, The University of British Columbia, Vancouver, BC V6T 1Z1, Canada*

Ryan P. Jansonius − *Department of Chemistry, The University of British Columbia, Vancouver, BC V6T 1Z1, Canada;* orcid.org/0000-0002-4014-2068

Noah J. J. Johnson − *Department of Chemistry, The University of British Columbia, Vancouver, BC V6T 1Z1, Canada*

Camden Hunt − *Department of Chemistry and Stewart Blusson Quantum Matter Institute, The University of British Columbia, Vancouver, BC V6T 1Z1, Canada*

Jingfu He − *Department of Chemistry, The University of British Columbia, Vancouver, BC V6T 1Z1, Canada*

Aiko Kurimoto − *Department of Chemistry, The University of British Columbia, Vancouver, BC V6T 1Z1, Canada*

Zishuai Zhang − *Department of Chemistry, The University of British Columbia, Vancouver, BC V6T 1Z1, Canada*

Complete contact information is available at: https://pubs.acs.org/10.1021/jacsau.0c00051

Notes

The authors declare no competing financial interest.

■ ACKNOWLEDGMENTS

The authors are grateful to the Canadian Natural Science and Engineering Research Council (RGPIN 337345-13; RGPIN-2017-03732), Canadian Foundation for Innovation (229288), Canadian Institute for Advanced Research (BSE-BERL-162173), and the Canada Research Chairs for financial support. This research was undertaken thanks in part to funding from the Canada First Research Excellence Fund, Quantum Materials, and Future Technologies Program. SEM imaging was performed in the Centre for High-Throughput Phenogenomics at the University of British Columbia, a facility supported by the Canada Foundation for Innovation, British Columbia Knowledge Development Foundation, and the UBC Faculty of Dentistry. We thank Derrick Horne for expert guidance on TEM analyses at the UBC Bioimaging facility. We thank Maureen Soon in the department of Earth, Ocean and Atmospheric Sciences at UBC for performing the ICP-OES.

■ REFERENCES

(1) Catalytic Hydrogenation and Dehydrogenation. In *Fine Chemicals through Heterogeneous Catalysis*; Sheldon, R. A., van Bekkum, H., Eds.; Wiley-VCH: Weinheim, New York, 2001.

(2) Ramachandran, R.; Menon, R. K. An overview of industrial uses of hydrogen. *Int. J. Hydrogen Energy* **1998**, *23*, 593−598.

(3) Deliy, I. V.; Simakova, I. L.; Ravasio, N.; Psaro, R. Catalytic behaviour of carbon supported platinum group metals in the hydrogenation and isomerization of methyl oleate. *Appl. Catal., A* **2009**, *357*, 170−177.

(4) Liu, L.; Corma, A. Metal catalysts for heterogeneous catalysis: from single atoms to nanoclusters and nanoparticles. *Chem. Rev.* **2018**, *118*, 4981−5079.

(5) Ruditskiy, A.; Peng, H.-C.; Xia, Y. Shape-controlled metal nanocrystals for heterogeneous catalysis. *Annu. Rev. Chem. Biomol. Eng.* **2016**, *7*, 327−348.

(6) Crespo-Quesada, M.; Yarulin, A.; Jin, M.; Xia, Y.; Kiwi-Minsker, L. Structure sensitivity of alkynol hydrogenation on shape- and size-controlled palladium nanocrystals: which sites are most active and selective? *J. Am. Chem. Soc.* **2011**, *133*, 12787−12794.

(7) Wilson, O. M.; Knecht, M. R.; Garcia-Martinez, J. C.; Crooks, R. M. Effect of Pd nanoparticle size on the catalytic hydrogenation of allyl alcohol. *J. Am. Chem. Soc.* **2006**, *128*, 4510−4511.

(8) Laskar, M.; Skrabalak, S. E. Decoupling the geometric parameters of shape-controlled Pd nanocatalysts. *ACS Catal.* **2014**, *4*, 1120−1128.

(9) Zhao, X.; Zhao, Y.; Fu, G.; Zheng, N. Origin of the facet dependence in the hydrogenation catalysis of olefins: experiment and theory. *Chem. Commun.* **2015**, *51*, 12016−12019.

(10) Azarpour, A.; Nejad Ghaffar Borhani, T.; Wan Alwi, S. R.; Abdul Manan, Z.; Madooli Behbehani, M. Prediction of Pd/C catalyst deactivation rate and assessment of optimal operating conditions of industrial hydropurification process. *Ind. Eng. Chem. Res.* **2015**, *54*, 7067−7082.

(11) Cao, S.; Tao, F. F.; Tang, Y.; Li, Y.; Yu, J. Size- and shape-dependent catalytic performances of oxidation and reduction reactions on nanocatalysts. *Chem. Soc. Rev.* **2016**, *45*, 4747−4765.

(12) Chen, S.; Wojcieszak, R.; Dumeignil, F.; Marceau, E.; Royer, S. How catalysts and experimental conditions determine the selective hydroconversion of furfural and 5-hydroxymethylfurfural. *Chem. Rev.* **2018**, *118*, 11023−11117.

(13) Zhang, L.; Zhou, M.; Wang, A.; Zhang, T. Selective hydrogenation over supported metal catalysts: from nanoparticles to single atoms. *Chem. Rev.* **2020**, *120*, 683−733.

(14) Bjelić, A.; Likozar, B.; Grilc, M. Scaling of lignin monomer hydrogenation, hydrodeoxygenation and hydrocracking reaction micro-kinetics over solid metal/acid catalysts to aromatic oligomers. *Chem. Eng. J.* **2020**, *399*, 125712.

(15) Bjelić, A.; Grilc, M.; Likozar, B. Bifunctional metallic-acidic mechanisms of hydrodeoxygenation of eugenol as lignin model compound over supported Cu, Ni, Pd, Pt, Rh and Ru catalyst materials. *Chem. Eng. J.* **2020**, *394*, 124914.

(16) Bjelić, A.; Grilc, M.; Huš, M.; Likozar, B. Hydrogenation and hydrodeoxygenation of aromatic lignin monomers over Cu/C, Ni/C, Pd/C, Pt/C, Rh/C and Ru/C Catalysts: mechanisms, reaction micro-kinetic modelling and quantitative structure-activity relationships. *Chem. Eng. J.* **2019**, *359*, 305−320.

(17) Schoenbaum, C. A.; Schwartz, D. K.; Medlin, J. W. Controlling the surface environment of heterogeneous catalysts using self-assembled monolayers. *Acc. Chem. Res.* **2014**, *47*, 1438−1445.

(18) Singh, U. K.; Vannice, M. A. Kinetics of liquid-phase hydrogenation reactions over supported metal catalysts—a review. *Appl. Catal., A* **2001**, *213*, 1−24.

(19) Pang, S. H.; Schoenbaum, C. A.; Schwartz, D. K.; Medlin, J. W. Directing reaction pathways by catalyst active-site selection using self-assembled monolayers. *Nat. Commun.* **2013**, *4*, 2448.

(20) Zhang, H.; Gu, X.-K.; Canlas, C.; Kropf, A. J.; Aich, P.; Greeley, J. P.; Elam, J. W.; Meyers, R. J.; Dumesic, J. A.; Stair, P. C.; Marshall, C. L. Atomic layer deposition overcoating: tuning catalyst selectivity for biomass conversion. *Angew. Chem., Int. Ed.* **2014**, *53*, 12132−12136.

(21) Mäki-Arvela, P.; Hájek, J.; Salmi, T.; Murzin, D. Y. Chemoselective hydrogenation of carbonyl compounds over heterogeneous catalysts. *Appl. Catal., A* **2005**, *292*, 1−49.

(22) Johnson, A. D.; Daley, S. P.; Utz, A. L.; Ceyer, S. T. The chemistry of bulk hydrogen: reaction of hydrogen embedded in nickel with adsorbed CH_3. *Science* **1992**, *257*, 223−225.

(23) Hansen, P. L.; Wagner, J. B.; Helveg, S.; Rostrup-Nielsen, J. R.; Clausen, B. S.; Topsøe, H. Atom-resolved imaging of dynamic shape

changes in supported copper nanocrystals. *Science* **2002**, *295*, 2053−2055.
(24) Teschner, D.; Borsodi, J.; Wootsch, A.; Revay, Z.; Havecker, M.; Knop-Gericke, A.; Jackson, S. D.; Schlogl, R. The roles of subsurface carbon and hydrogen in palladium-catalyzed alkyne hydrogenation. *Science* **2008**, *320*, 86−89.
(25) Gallezot, P.; Richard, D. Selective hydrogenation of α,β-unsaturated aldehydes. *Catal. Rev.: Sci. Eng.* **1998**, *40*, 81−126.
(26) Sherbo, R. S.; Delima, R. S.; Chiykowski, V. A.; MacLeod, B. P.; Berlinguette, C. P. Complete electron economy by pairing electrolysis with hydrogenation. *Nat. Catal.* **2018**, *1*, 501−507.
(27) Jansonius, R. P.; Kurimoto, A.; Marelli, A. M.; Huang, A.; Sherbo, R. S.; Berlinguette, C. P. Hydrogenation without H_2 using a palladium membrane flow cell. *Cell Reports Physical Science* **2020**, *1*, 100105.
(28) Wicke, E.; Brodowsky, H.; Züchner, H. Hydrogen in Palladium and Palladium Alloys. In *Hydrogen in Metals II: Application-Oriented Properties*; Alefeld, G., Völkl, J.,, Eds.; Springer Berlin Heidelberg: Berlin, Heidelberg, 1978; pp 73−155.
(29) Yan, B.; Bisbey, R. P.; Alabugin, A.; Surendranath, Y. Mixed electron−proton conductors enable spatial separation of bond activation and charge transfer in electrocatalysis. *J. Am. Chem. Soc.* **2019**, *141*, 11115−11122.
(30) Mukherjee, D. Potential application of palladium nanoparticles as selective recyclable hydrogenation catalysts. *J. Nanopart. Res.* **2008**, *10*, 429−436.
(31) Lopez-Sanchez, J. A.; Dimitratos, N.; Hammond, C.; Brett, G. L.; Kesavan, L.; White, S.; Miedziak, P.; Tiruvalam, R.; Jenkins, R. L.; Carley, A. F.; Knight, D.; Kiely, C. J.; Hutchings, G. J. Facile removal of stabilizer-ligands from supported gold nanoparticles. *Nat. Chem.* **2011**, *3*, 551−556.
(32) Monzó, J.; Koper, M. T. M.; Rodriguez, P. Removing polyvinylpyrrolidone from catalytic Pt nanoparticles without modification of superficial order. *ChemPhysChem* **2012**, *13*, 709−715.
(33) Luo, M.; Hong, Y.; Yao, W.; Huang, C.; Xu, Q.; Wu, Q. Facile removal of polyvinylpyrrolidone (PVP) adsorbates from Pt alloy nanoparticles. *J. Mater. Chem. A* **2015**, *3*, 2770−2775.
(34) Johnson, N. J. J.; Lam, B.; Sherbo, R. S.; Fork, D. K.; Berlinguette, C. P. Ligands affect hydrogen absorption and desorption by palladium nanoparticles. *Chem. Mater.* **2019**, *31*, 8679−8684.
(35) Kurimoto, A.; Sherbo, R. S.; Cao, Y.; Loo, N. W. X.; Berlinguette, C. P. Electrolytic deuteration of unsaturated bonds without Using D_2. *Nat. Catal.* **2020**, *3*, 719−726.
(36) Cantu, D. C.; Padmaperuma, A. B.; Nguyen, M.-T.; Akhade, S. A.; Yoon, Y.; Wang, Y.-G.; Lee, M.-S.; Glezakou, V.-A.; Rousseau, R.; Lilga, M. A. A combined experimental and theoretical study on the activity and selectivity of the electrocatalytic hydrogenation of aldehydes. *ACS Catal.* **2018**, *8*, 7645−7658.
(37) Liu, W.; You, W.; Gong, Y.; Deng, Y. High-efficiency electrochemical hydrodeoxygenation of bio-phenols to hydrocarbon fuels by a superacid-noble metal particle dual-catalyst system. *Energy Environ. Sci.* **2020**, *13*, 917−927.
(38) Bhanushali, J. T.; Kainthla, I.; Keri, R. S.; Nagaraja, B. M. Catalytic hydrogenation of benzaldehyde for selective synthesis of benzyl alcohol: a review. *ChemistrySelect* **2016**, *1*, 3839−3853.
(39) Lim, B.; Jiang, M.; Tao, J.; Camargo, P. H. C.; Zhu, Y.; Xia, Y. Shape-controlled synthesis of Pd nanocrystals in aqueous solutions. *Adv. Funct. Mater.* **2009**, *19*, 189−200.
(40) Jin, M.; Liu, H.; Zhang, H.; Xie, Z.; Liu, J.; Xia, Y. Synthesis of Pd nanocrystals enclosed by {100} facets and with sizes < 10 nm for application in CO oxidation. *Nano Res.* **2011**, *4*, 83−91.
(41) Zalineeva, A.; Baranton, S.; Coutanceau, C.; Jerkiewicz, G. Electrochemical behavior of unsupported shaped palladium nanoparticles. *Langmuir* **2015**, *31*, 1605−1609.
(42) Wan, J.; Kim, Y.; Mulvihill, M. J.; Tokunaga, T. K. Dilution destabilizes engineered ligand-coated nanoparticles in aqueous suspensions. *Environ. Toxicol. Chem.* **2018**, *37*, 1301−1308.
(43) Hattori, K.; Sajiki, H.; Hirota, K. Chemoselective control of hydrogenation among aromatic carbonyl and benzyl alcohol derivatives using Pd/C(en) catalyst. *Tetrahedron* **2001**, *57*, 4817−4824.
(44) Nalajala, N.; Gooty Saleha, W. F.; Ladewig, B. P.; Neergat, M. Sodium borohydride treatment: a simple and effective process for the removal of stabilizer and capping agents from shape-controlled palladium nanoparticles. *Chem. Commun.* **2014**, *50*, 9365−9368.
(45) Morgenstern, M.; Michely, T.; Comsa, G. Anisotropy in the adsorption of H_2O at low coordination sites on Pt (111). *Phys. Rev. Lett.* **1996**, *77*, 703−706.
(46) Jakub, Z.; Hulva, J.; Meier, M.; Bliem, R.; Kraushofer, F.; Setvin, M.; Schmid, M.; Diebold, U.; Franchini, C.; Parkinson, G. S. Local structure and coordination define adsorption in a model Ir_1/Fe_3O_4 single-atom catalyst. *Angew. Chem.* **2019**, *131*, 14099−14106.
(47) Niu, Z.; Li, Y. Removal and utilization of capping agents in nanocatalysis. *Chem. Mater.* **2014**, *26*, 72−83.

https://dx.doi.org/10.1021/jacsau.0c00051
JACS Au 2021, 1, 336−343